

QuantSR+: Pushing the Limit of Quantized Image Super-Resolution Networks

Haotong Qin, Xudong Ma, Xianglong Liu, *Senior Member, IEEE*, Jie Luo, Jinyang Guo, Michele Magno, *Fellow, IEEE*, Yulun Zhang*

Abstract—Low-bit quantization is widely used to compress super-resolution (SR) models and reduce storage and computation costs for deployment on resource-limited devices. However, when SR models are pushed to ultra-low precision (2-4 bits), performance can drop sharply due to diminished representational capacity and the detail-sensitive nature of SR. To address these issues, we propose **QuantSR+**, a unified framework that improves quantization operators, network design, and training optimization, achieving better trade-offs between accuracy and efficiency than prior low-bit SR methods. QuantSR+ mainly relies on three technical contributions: (1) *Redistribution-driven Bit Determination* (RBD), which reshapes quantization distributions in both forward and backward passes to preserve representation fidelity; (2) *Quantized Slimmable Architecture* (QSA), which begins with an over-parameterized model and progressively prunes less critical blocks to meet efficiency budgets while pushing the accuracy performance; and (3) *Slimming-guided Function-localized Distillation* (SFD), which enforces block-aware feature alignment via a direct loss and a progressive, function-local training schedule to capture quantization effects better and speed up convergence. Extensive experiments show that QuantSR+ achieves state-of-the-art performance against both specialized quantized SR methods and generic quantization approaches. For SwinIR-S on Urban100 ($\times 4$), it improves PSNR by 0.29 dB over the 2-bit SOTA baseline. Meanwhile, it delivers strong efficiency gains at 2-bit, reducing operations by up to 87.9% and storage by 89.4%. QuantSR+ is effective for both convolutional and transformer-based SR models, indicating broad applicability. Code and pretrained models are available [here](#).

Index Terms—Low-Bit Quantization, Model Compression, Image Super-Resolution, Deep Learning, Computer Vision



1 INTRODUCTION

WITH the rapid development of deep neural networks, the demand for image super-resolution (SR) applications is widespread across various scenarios [26], [34]. The SR task aims to reconstruct a high-resolution (HR) version from a low-resolution (LR) input by inferring high-frequency details, but it is inherently ill-posed because an LR image may correspond to multiple possible HR candidates [12], [36], [44], [46], [63]. Existing efforts typically focus on convolution-based or transformer-based network designs to achieve high reconstruction fidelity [35], [58], [60], and recent diffusion-based SR further improves the perceptual quality of SR reconstruction [52], [56]. Due to the large volume of parameters and high computational complexity, current image SR models often demand costly hardware resources for real-time deployment, posing challenges in resource-constrained scenarios such as mobile or edge devices. Therefore, model compression approaches are urgently needed to achieve lightweight models and efficient inference. Among various compression approaches, low-bit quantization effectively compresses and accelerates models by reducing parameter bit-width: by quantizing computation-intensive units such as convolutions, matrix multiplications, and linear layers [7], [20], [22], [45], [49], quantized models can use efficient integer operations instead of floating-point computations, which is particularly important for deploying advanced artificial intelligence applications on edge devices; moreover, quantization mainly compresses parameters within layers

on an element-wise basis, making it widely applicable across architectures and tasks, and the quantization function (quantizer) can be customized to specific bit-widths, typically 2 to 8 bits, to flexibly balance accuracy and efficiency [19], [39], [47], [51], [53], [61].

Although low-bit weights and activations can enhance computational efficiency, quantization may significantly degrade or even destabilize performance in image SR tasks, especially when employing ultra-low bit-widths, *e.g.*, 2-4 bits. While existing studies have attempted to minimize quantization losses, a considerable performance gap remains between low-bit SR models and their full-precision counterparts. We attribute this performance degradation primarily to the following three factors: (1) **Operator Degradation**: Particularly in ultra-low bit-width quantization, the bit-wise discretization process results in highly degraded and inaccurate representations within the computation units of SR models, limiting the quality and diversity of the output of the SR model. (2) **Structure Constraints**: Since quantization occurs at the parameter level, the accuracy of the full-precision model with the same structure can almost be seen as the upper limit for the quantized versions, making it challenging to reach an optimal solution in the discrete parameter space. (3) **Optimization Perturbations**: The quantization errors introduced during discretization are difficult to estimate directly and tend to accumulate during training, thereby complicating the stable convergence of quantized SR models.

To address these challenges encountered in low-bit quantization, we propose an accurate, efficient, and flexible **Quantized image Super-Resolution model, QuantSR+**,

- H. Qin and M. Magno are from ETH Zurich, Switzerland. Y. Zhang (*Corresponding Author, E-mail: yulun100@gmail.com) is from Shanghai Jiao Tong University, China. X. Ma, X. Liu, J. Luo, and J. Guo are from Beihang University, China.

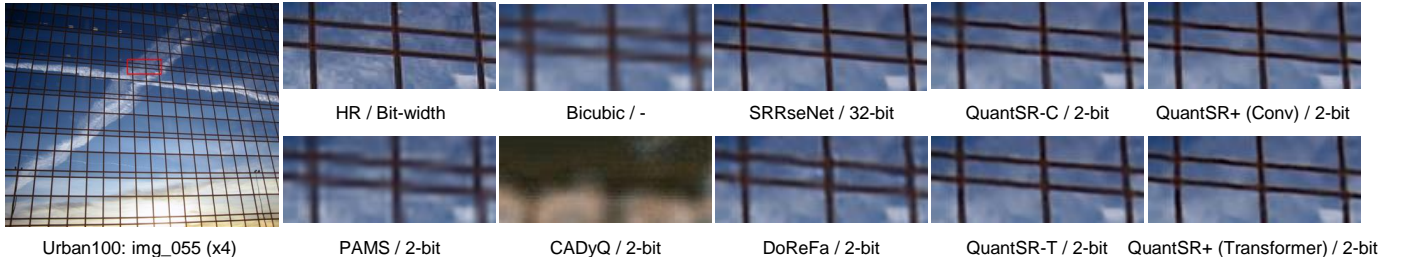


Fig. 1: Visualization for quantized SR models in Urban100 $\times 4$ scale, and SRRseNet [28] is used as the full-precision SR model. QuantSR+ outperforms recent quantization methods consistently, including DoReFa [65], PAMS [31], CADyQ [16], and QuantSR [43].

designed to push the performance of SR models under low bit-widths to the limit. At the operator level, we introduce *Redistribution-driven Bit Determination* (RBD), which optimizes and reconstructs bit-level quantization function representations during both forward and backward propagation through propagation-based redistribution. Compared to vanilla quantization, RBD enhances the accuracy of quantized units within the SR model without increasing the inference overhead through bit-level reorganization. At the structure level, we develop the *Quantized Slimmable Architecture* (QSA), which starts from an over-parameterized initial structure that is two times larger than the targeted compressed model. It aims to push the upper accuracy limits of compressed models. It allows for progressive structural evolution during training, intending to surpass the accuracy set by the original counterparts under specific inference efficiency constraints. At the optimization level, we implement *Slimming-guided Function-localized Distillation* (SFD), which introduces a direct loss to capture quantization effects and a progressive strategy for optimizing network blocks based on their local functions. By adjusting the granularity of internal feature alignment, SFD effectively supervises the quantized SR model, ensuring both stability and faster convergence.

We conduct extensive experiments to demonstrate that the performance of QuantSR+ significantly surpasses various bit-width quantized SR models (see Fig. 1), with 2-bit QuantSR+ performing comparably to existing state-of-the-art methods using 4 bits. We also verified the versatility of QuantSR+ on convolutional and transformer-based SR networks, along with its theoretical and deployment efficiency, showcasing its adaptability across different tasks, architectures, and scenarios. Comprehensive quantization and visualization results show that QuantSR+ surpasses current state-of-the-art quantized SR networks and general quantization approaches, achieving a significant improvement of 0.29 dB in PSNR over 2-bit existing SOTA methods on the $\times 4$ Urban100 dataset. QuantSR+ demonstrates comprehensive accuracy and efficiency enhancements across both convolutional and transformer-based architectures, validating the versatility of the proposed techniques in various architectures. QuantSR+ can also achieve exceptional computational efficiency. We report the inference efficiency of 4-bit and 2-bit QuantSR+, and the 2-bit version even achieves an 87.9% reduction of computational FLOPs and 88.2% reduction of storage usage compared to its full-precision counterpart.

Note that the paper is an extension of the original conference version [43]. Compared with the conference

version, the main contributions of the paper are

- This paper further identifies the causes of significant performance degradation of quantized SR models at ultra-low bit-widths, comprehensively pointing out the issues from operator degradation, structure constraints, and optimization perturbations as the primary challenges faced by quantized SR models. This provides empirical inspiration for QuantSR+.
- We propose QuantSR+, an accurate and efficient algorithm designed to push the performance of low-bit super-resolution models to their limits. In particular, we emphasize that QuantSR+ introduces comprehensive improvements over the original conference paper in both the quantizer design and the model architecture, and further presents a new distillation-based optimization strategy. As a result, compared with the method in the original conference version, QuantSR+ offers stronger representational capacity and is easier to optimize:
 - (1) We improve the quantizer via bit-determination redistribution. Compared with the conference paper, this technique refines redistribution in the weight quantizer down to the individual-bit level, improving the flexibility and accuracy of the quantized representation. More importantly, the packed quantized weights produced by the quantizer are exactly consistent with standard integers and so incur no additional inference overhead.
 - (2) We improve the quantized architecture to break through its accuracy limits. Unlike the conference paper, which abruptly changes the entire architecture at a certain point, this technique distributes the slimming process across blocks and stages of training. It better couples architectural evolution with the training procedure, enabling the quantized model to be continuously optimized throughout training.
 - (3) We propose a novel function-localized distillation for quantization-aware training. Compared with the standard training pipeline used in the conference version, this technique introduces a distillation loss based on localized functional reconstruction, allowing targeted optimization of the slimmed quantized architecture. It helps the quantized model remain stable during slimming evolution and converge faster.
- Further detailed evaluations and analyses of the quantized SR networks are presented, including more quantitative and visual results for image SR tasks and statistical analysis of parameters during training, showcasing the significant accuracy and efficiency improvements brought by QuantSR+. We also report the compu-

tational Ops and storage savings of the proposed QuantSR+, demonstrating its efficiency potential in resource-constrained scenarios. The results show that significant accuracy improvements are achieved without additional efficiency, which strongly demonstrates the advantages of QuantSR+ over existing methods.

2 RELATED WORK

2.0.1 Efficient Image SR Model

Convolutional neural networks have consistently exhibited remarkable performance in image SR. EDSR [34] and SRResNet [28] already outperformed traditional methods and have since served as a pivotal CNN-based reference. Vision Transformers (ViT) [10] have catalyzed the emergence of Transformer-driven approaches, exemplified by SwinIR [33], which surpass many CNN models. Meanwhile, efficiency-oriented strategies such as Neural Architecture Search (NAS) [4], Knowledge Distillation (KD) [15], and pruning [13] have been broadly investigated to address resource constraints. Efforts include multi-distillation networks to mitigate redundancy [23], cascading residual networks for enhanced efficiency [1], and NAS-based approaches like FALSr [8]. KD has been adopted to train lightweight SR models [14], [30], while pruning, as in the ASSL framework [64], systematically removes surplus parameters. Although these methods are effective, they can overlook subtle redundancies of computation and storage caused by the expensive floating-point parameters in networks. Consequently, low-bit quantization stands out as a promising compression approach for shrinking bit-width and computational costs while sustaining performance in real-world SR applications.

2.0.2 Model Quantization

Among the various quantization techniques, Quantization-Aware Training (QAT) [19], [47], [53], [65] and Post-Training Quantization (PTQ) [22], [49], [51] have emerged as the primary approaches for reducing computational and memory overhead in deep neural networks [5], [11]. QAT incorporates quantization directly into the training process, thus leveraging rich training signals to support aggressive low-bit (2-4 bits) quantization [6], [16], [31], [65]. By fine-tuning parameters while accounting for quantization effects, QAT enables substantial efficiency gains while mitigating accuracy degradation. In contrast, PTQ allows for quantizing pre-trained models without further training [22], offering a more straightforward and widely adopted approach [7], [22], [25]. Despite its simplicity, PTQ tends to underperform at extremely low bit widths due to its reliance on fixed parameters and the absence of retraining or fine-tuning. These limitations become pronounced when models are compressed to ultra-low-bit configurations.

2.0.3 Quantized SR Models

For SR tasks, low-bit quantization presents an effective approach to address the computational bottlenecks associated with high-resolution input data. SR models notoriously demand considerable floating-point operations and storage, making them prime candidates for compression strategies that can alleviate resource constraints [24], [37], [50]. As a result, researchers began to explore QAT-based

methods [19], [47], [53] to balance efficiency and accuracy in SR networks. Hong et al. proposed a distribution-aware quantization (DAQ) method that applies channel-wise, data-driven quantization parameters [18], while CADyQ employs a strategic bit-allocation scheme across different layers and image regions [16]. Similarly, PAMS leverages a trainable truncated parameter to dynamically adjust the upper bound of the quantization range, bolstering flexibility and performance [31]. Despite these advances, a notable performance gap remains between fully quantized SR models and their full-precision counterparts. Bridging this gap continues to be a critical research focus, as fully harnessing the benefits of low-bit quantization is essential for practical SR applications on resource-constrained devices.

3 METHOD

This section introduces the proposed **QuantSR+** for accurate and efficient image SR tasks. Firstly, we present the existing baselines for quantizing SR models, including the architecture definition of SR models as well as the quantization and computation processes. Subsequently, we detail the novel techniques in QuantSR+ to address various limitations of the existing baselines, including *Redistribution-driven Bit Determination* (RBD), *Quantized Slimmable Architecture* (QSA), and *Slimming-guided Function-localized Distillation* (SFD). Finally, we present how to apply QuantSR+ to image SR tasks and discuss the training pipeline and specific implementation details for quantized SR models.

3.1 Preliminaries

3.1.1 Architecture of Image SR Baseline

The architecture of quantized SR models is initiated by discussing its principal components. These models are designed to accept a low-resolution image, referred to as I_{LR} , and output a high-resolution counterpart, designated as I_{SR} . This transformation is mathematically encapsulated by:

$$I_{SR} = \mathcal{M}(I_{LR}), \quad (1)$$

where $\mathcal{M}(\cdot)$ symbolizes the quantized SR model. The model $\mathcal{M}(\cdot)$ typically integrates three key elements: a low-level feature extractor $\mathcal{E}_L(\cdot)$, a high-level feature extractor $\mathcal{E}_H(\cdot)$, and a reconstruction module $\mathcal{R}(\cdot)$. The high-level feature extractor, which is the primary target for quantization [31], is the most computationally intensive component of the network. The operational framework of the SR process, as previously defined, can be restructured as:

$$I_{SR} = \mathcal{R} \circ \mathcal{E}_H \circ \mathcal{E}_L(I_{LR}), \quad (2)$$

where \mathcal{E}_H denotes the high-level feature extractor, and \circ indicates the sequential composition of model parts.

3.1.2 Low-bit Quantization Framework

In image SR models employing quantization, both weights w and activations a are condensed into reduced bit-width representations via respective quantizers, *i.e.*, $Q_w(w)$ and $Q_a(a)$. This quantization commonly adopts a symmetric approach where the quantizers operate at a bit-width b , formulated as [55]:

$$Q_x^b(x) = \left[\text{clip} \left(\frac{x}{v_x^b}, -1, 1 \right) \right] \times v_x^b, \quad (3)$$

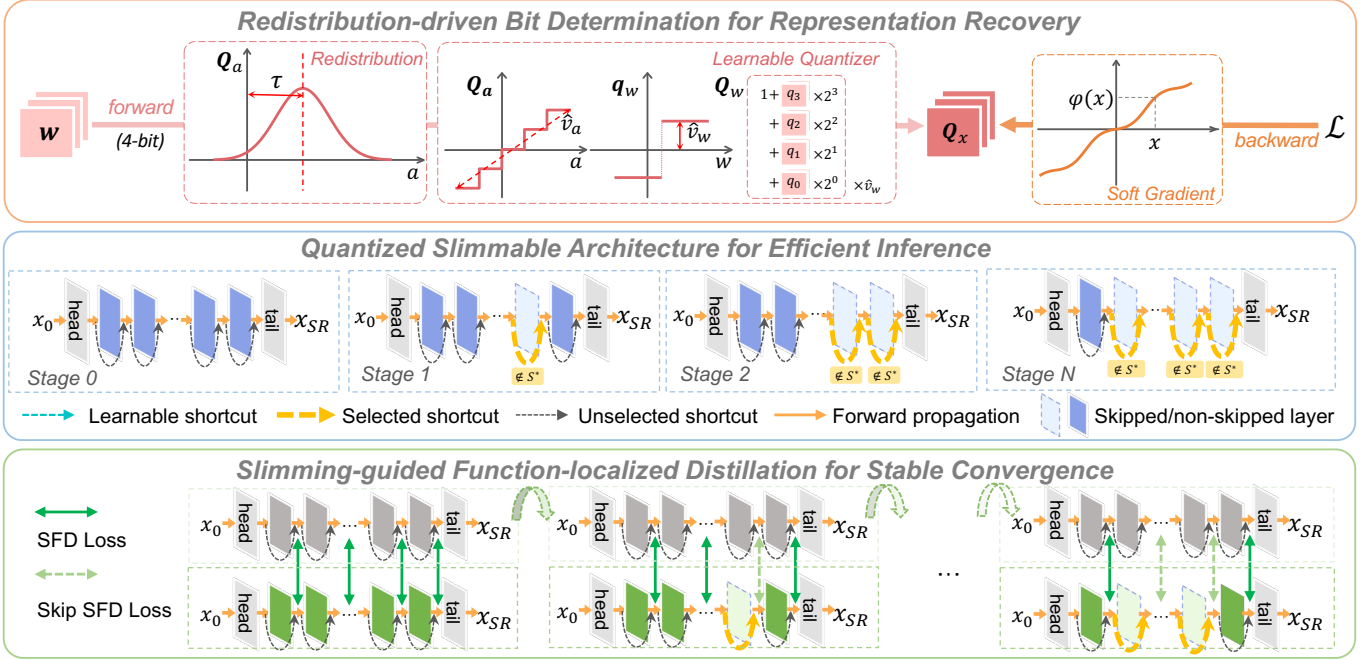


Fig. 2: Overview of the proposed QuantSR+ for image SR. The QuantSR+ improves the quantized SR network at the operator (RBD), structure (QSA), and optimization (SFD) levels comprehensively.

where x denotes the latent weight w or activation a , the clipping function $\text{clip}(\cdot, -1, 1) = \max(\min(\cdot, 1), -1)$ restricts the input range. Here, v_x^b serves as the scaling factor, transforming higher precision values to their quantized lower bit-width equivalents, defined by $v_x^b = \frac{2^{\max(|x|)}}{2^{b-1}}$. The main computation of the quantized unit can be expressed as

$$o = Q_w^b(w) \otimes Q_a^b(a), \quad (4)$$

where o denotes the output and \otimes denotes the convolution or linear projection composed of integer instructions. Due to the non-differentiability of the quantizer, which would result in zero gradients and thereby hinder the backward propagation, the gradient approximation through straight-through estimation (STE) [2] is utilized:

$$\frac{\partial Q^b(x)}{\partial x} = \begin{cases} 1 & \text{if } x \in (-r_x, r_x) \\ 0 & \text{otherwise} \end{cases}. \quad (5)$$

Quantization in image SR models significantly reduces storage demands and computational burden by lowering bit widths and optimizing integer operations, thus enhancing operational efficiency.

3.2 QuantSR+: Redistribution-driven Bit Determination

3.2.1 Quantization-induced Operator Degradation

The quantization approach compresses weights and activations of models to low-bit representations for compact storage and accelerated computation, thus benefiting efficiency. However, quantization also results in a significant drop in accuracy in image SR tasks, especially when reducing model precision to ultra-low bit-widths (2-4 bits). Specifically, the primary cause of this phenomenon is the high level of discretization introduced by the quantization function, which affects both the forward and backward propagation.

During forward propagation, quantization makes feature representations much more discrete and less diverse, which can limit how precisely an SR network encodes fine-grained image details. For instance, moving from 32-bit floating-point to 2-bit quantization reduces the per-element value space from 2^{32} to 2^2 , creating an enormous representational gap of about 2^{30} (roughly one billion) times. During backward propagation, quantizers are non-differentiable because they contain rounding and clipping operations. Therefore, training uses the straight-through estimator (STE) [2], which replaces the true derivative of the quantizer with an identity or clipped identity function. This surrogate gradient ignores quantization bin boundaries and assigns non-zero gradients even where the forward mapping is piecewise constant and has zero true derivative almost everywhere. As a result, the backward gradient is biased with respect to the true sensitivity of the quantized forward operator, creating a systematic forward-backward inconsistency. In low-bit SR settings, where quantization intervals are coarse, this inconsistency becomes more pronounced and can delay parameter updates from matching the true sensitivity changes that occur when activations or weights cross quantization bin boundaries, which directly affects reconstruction fidelity. Since STE is required for practical optimization of non-differentiable quantizers, this mismatch cannot be fully removed and must instead be mitigated by better quantization-aware training.

3.2.2 Redistribution-driven Bit Determination for Representation Recovery

In this work, we introduce a novel Redistribution-driven Bit Determination (RBD) method for QuantSR+ (see Fig. 3). RBD stems from a straightforward motivation: to extremely fine-grain the forward and backward processes of quantization, building redistribution-driven quantizers at the single-bit level. During inference, RBD doesn't introduce any overhead

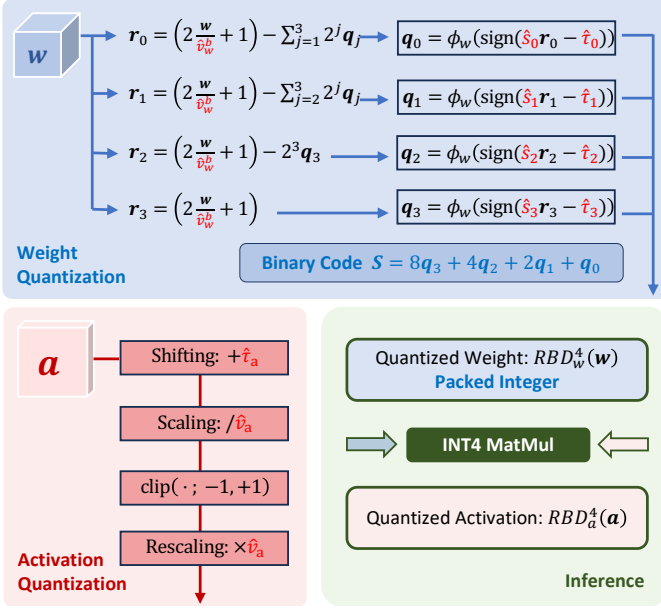


Fig. 3: Training and inference processes of 4-bit RBD. Red notations are learnable parameters in RBD quantizers.

and is fully consistent with standard hardware quantization operators. Ultimately, it facilitates accurate and flexible model optimization in SR tasks.

3.2.2.1 RBD in Weight Quantization: In weight quantization, RBD introduces a learnable redistribution mechanism, *i.e.*, a set of trainable parameters that control how much each binary bit contributes to the final quantized value. Specifically, it does **not** redistribute the original weight distribution directly; instead, it learns the relative contribution of different bit planes when composing an b -bit code. To this end, we reconstruct the weight quantizer by explicitly combining multiple binary bits into an b -bit integer-equivalent representation. Given a full-precision weight tensor w , the b -bit quantized weight $RBD_w^b(w)$ can be equivalently written as a weighted sum of b binary bits with a shared channel-wise scaling factor. The formulation is

$$RBD_w^b(w) = \frac{1}{2} (S - 1) \hat{v}_w, \quad S = \sum_{i=0}^{b-1} 2^i q_i, \quad (6)$$

where $q_i \in \{-1, 1\}$ denotes the i -th bit obtained by the sign function. \hat{v}_w is a learnable channel-wise scaling factor that aligns the magnitude of the discrete codebook to that of the full-precision weights. We initialize \hat{v}_w by matching the mean absolute value between w and the integer code S , *i.e.*,

$$\hat{v}_w \leftarrow \frac{2 \mathbb{E}(|w|)}{\mathbb{E}(|S - 1|)}, \quad (7)$$

where $\mathbb{E}(\cdot)$ denotes the channel-wise average.

Then, we design redistribution-driven determination functions for each bit. Specifically, we determine the i -th bit from a residual signal constructed in the integer-code domain. By removing the contributions of the already-determined higher bits, each decision focuses on the remaining quantiza-

tion error. The proposed residual-driven bit determination can be written as:

$$r_i = \left(2 \frac{w}{\hat{v}_w} + 1\right) - \sum_{j=i+1}^{b-1} 2^j q_j, \quad (8)$$

$$q_i = \text{sign}(\phi_w(\hat{s}_i r_i - \hat{t}_{w,i})). \quad (9)$$

where r_i denotes the residual before deciding q_i in the integer-code domain. It is obtained by first mapping the normalized weight to $\left(2 \frac{w}{\hat{v}_w} + 1\right)$, which is consistent with the form in Eq. (6). Then it subtracts the reconstructed contribution of higher bits $\{q_j\}_{j>i}$. \hat{v}_w , \hat{s} , and \hat{t}_w are all learnable parameters. \hat{v}_w adjusts the overall range of w , while \hat{s} and \hat{t}_w regulate the distribution of the latent weights when determining each bit, initialized as 1 and 0, respectively. By conditioning each bit on r_i , the quantizer performs an explicit residual refinement: higher bits explain the dominant component first, and lower bits progressively compensate the remaining residual. Simultaneously, the uniform application of the sign function yields a consistent post-discretization representation, so the resulting quantized outputs are equivalent to integer-quantized values and can be computed efficiently using standard integer instructions during inference.

We also introduce an embedded transformation function $\phi_w(\cdot)$ before the discretization in each bit determination function. The forward and backward processes are

$$\phi_w(x) = \tanh(2x), \quad \partial \phi_w(x) / \partial x = 2 \text{sech}^2(2x), \quad (10)$$

where x denotes the input to the external $\text{sign}(\cdot)$ operator. Since $\tanh(\cdot)$ is strictly monotonic and odd, it preserves the sign of non-zero inputs, *i.e.*, $\text{sign}(\phi_w(x)) = \text{sign}(x)$. In backward propagation, $2 \text{sech}^2(2x)$ smoothly down-weights gradients for elements with large $|x|$ that are far from the decision boundary, while maintaining well-defined, non-zero gradients for finite inputs. This encourages stable optimization by focusing updates on the latent weights that are more likely to affect the discretized bit decisions, thereby better reflecting the forward quantization behavior.

3.2.2.2 RBD in Activation Quantization: For the quantization of activations, the ongoing variation between different propagation cycles during inference results in computationally expensive per-bit decisions. Therefore, we treat the quantizer for activations as an integrated integer quantizer, which is defined as follows:

$$RBD_a^b(a) = \lfloor \phi_a(\text{clip}((a + \hat{t}_a) / \hat{v}_a, -1, 1)) \rfloor \times \hat{v}_a, \quad (11)$$

where \hat{v}_a and \hat{t}_a denote learnable scaling factors and mean-shifts for quantized activations, respectively, which are both learnable parameters. The formulation allows the activation quantizer to adaptively adjust the range and granularity of the quantization intervals, leveraging redistribution to preserve the diversity of the activations and ensure accurate representation even at lower bit widths:

$$\phi_a(a) = \tanh(2(a - \lfloor a \rfloor) - 1) / \tanh(1) + \lfloor a \rfloor + 1, \quad (12)$$

$$\partial \phi_a(a) / \partial a = 2 \text{sech}^2(2(a - \lfloor a \rfloor) - 1) / \tanh(1). \quad (13)$$

This function does not alter the rounding value, but mitigates the gradient of elements distant from the center within each

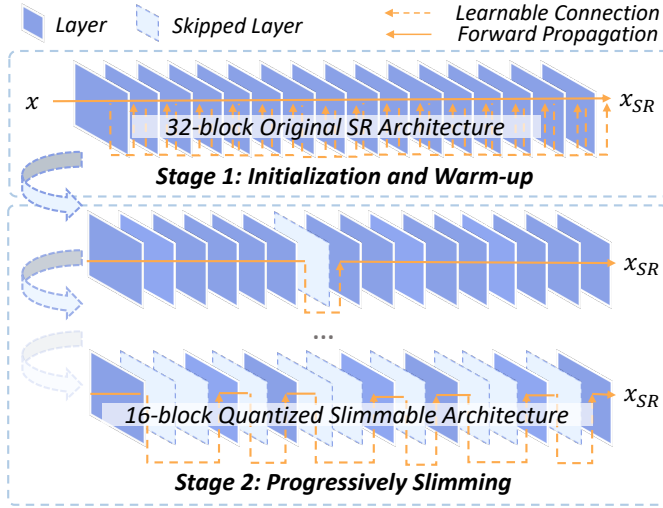


Fig. 4: The illustration of QSA. A dual-stage approach is applied to progressively slim and optimize the quantized SR model.

interval. It thus better reflects the quantization behavior and achieves more accurate yet stable gradients.

The proposed RBD quantizer improves quantized weights and activations in both forward and backward propagation. In the **forward pass**, bit decisions are modulated by learnable redistribution parameters, which adapt the contribution of each bit plane during training and yield accurate yet flexible low-bit representations. Notably, the resulting discrete representations are inherently integer-equivalent under the bit-composition form in Eq. (6), and thus can be directly realized by standard integer quantization operators for deployment. In the **backward pass**, the embedded transformation functions $\phi_w(\cdot)$ and $\phi_a(\cdot)$ provide smooth, content-aware surrogate gradients. Compared with a plain STE, this design down-weights gradients for elements far from decision boundaries, leading to more stable and effective parameter updates without adding inference overhead. During **inference**, the integer-equivalent weights $RBD_w^b(w)$ and quantized activations $RBD_a^b(a)$ are multiplied using integer arithmetic for efficient execution.

3.3 QuantSR+: Quantized Slimmable Architecture

3.3.1 Constraints from Latent Structures

As a model compression method utilizing low-bit parameters and computations, quantization enables efficient inference of SR models on resource-constrained hardware. Specifically, one of the main advantages of quantization is its universality regarding the bit-width of parameters in the model. This means it is adaptable to diverse architectures, thus enabling the compression of various SR models without altering their fundamental structures.

However, the architectural universality of quantization also introduces two key limitations for quantized SR models. First, the performance ceiling is often bounded by the full-precision counterpart with the same fixed structure and parameter budget, inevitably leaving an accuracy gap. Second, quantization alone does not remove structural redundancy, implying that more compact structures may exist under the same accuracy target. Our conference version, QuantSR [43],

has explored slimming, but it adopts a one-shot slimming at a specific point during training. This abrupt change in network topology can perturb optimization, and it may also invalidate part of the optimization progress accumulated before slimming, since the pre-slim parameters/representations cannot be consistently aligned with the post-slim architecture.

To address these issues, QuantSR+ introduces a Quantized Slimmable Architecture (QSA) that evolves progressively during training, rather than shrinking the model in a single step. By warm-starting from an over-parameterized quantized network with learnable shortcuts and then gradually skipping less important blocks, QSA preserves training continuity, reuses previously learned representations, and yields a more stable optimization path toward the final slim and efficient architecture.

3.3.2 Quantized Slimmable Architecture for Efficient Inference

We introduce the Quantized Slimmable Architecture (QSA) for QuantSR+, specifically tailored for the advanced feature extractor \mathcal{E}'_H in quantized SR models (see Figure 4). Compared with the previous methods with direct quantization or one-shot slimming, the proposed QSA further pushes the limit of the representation capacity from a structure perspective to achieve higher accuracy.

Our first step is to construct the initialization of the slimmable architecture. The vast majority of mainstream architectures used for SR tasks, including convolution-based [28] and transformer-based [33] models, consist of several computational blocks of the same size. Considering their quantization-aware training process, the latent weights in different blocks of the model exhibit varying sensitivities to quantization [9], [25], and extracted features have different levels of importance for prediction. Therefore, we first construct an initial setting for the quantized SR model with twice the number of blocks, allowing it to surpass the original scale’s accuracy upper limit after quantization. This structure is based on quantized blocks accompanied by learnable shortcut connections, represented as \mathcal{E}^{QSA}_H , composed of $2N$ blocks ($N \in \{2^n, n \in \mathbf{Z}^+\}$), where the initial configuration of the i -th block $\Phi_i^{QSA}(\cdot)$ is described as follows:

$$\Phi_i^{QSA}(x_i) = \varphi_i(x_i) + \alpha_i x_i, \quad (14)$$

where x_i represents the input features of the i -th block, $\varphi(\cdot)$ denotes the quantized feature extractor consisting of convolutional and activation layers, and α is the learnable scaling factor of the shortcut connections. We perform a warm-up process for the constructed initial architecture, which only accounts for 20% of the total number of iterations in the training process. During the warm-up phase, $\varphi_i(\cdot)$ within $\Phi_i^{QSA}(\cdot)$ undergoes task-oriented optimization, while α_i is also updated during the learning process. Throughout the model, a lower α_i implies that the corresponding block’s computation is more difficult to disregard, signifying its greater importance within the entire quantized architecture.

Following initialization, QSA tightly integrates slimming with quantization-aware training and evolves the architecture in a progressive manner, rather than switching the network to a final slim topology at a specific stage [43]. Specifically, after the warm-up phase, we iteratively skip the blocks

with the highest α (remove them from the set S) and continue training the resulting student until it recovers the pre-slim accuracy. The skipped blocks of QSA will be removed in deployed inference. This procedure is repeated until the target efficiency constraint is satisfied (e.g., retaining N blocks, i.e., skipping 50% blocks), yielding a final architecture that is reached smoothly through successive intermediate states. The final QSA structure can be represented as:

$$\mathcal{E}_H^{\text{QSA}}(x, S^*) = \prod_{i=1}^{2N} \left[\Phi_i^{\text{QSA}} \in S^* \right] \Phi_i^{\text{QSA}}(x_i) + \left[\Phi_i^{\text{QSA}} \notin S^* \right] x_i, \quad (15)$$

where $[\cdot]$ denotes the Iverson bracket, equaling 1 if the condition inside the bracket is true, S^* represents the set of blocks not skipped in the final slim architecture, and \prod denotes the sequential combination of quantized blocks within the network. After the evolution of the structure, we train the resulting QSA until the complete quantization-aware training process concludes. In practice, we cap the number of iterations for each intermediate evolutionary state to avoid stalling at a state that fails to satisfy the target constraints. Specifically, the iteration budget for each state is set to $\frac{1}{N} \times 80\%$ of the total number of iterations.

QSA makes QuantSR+ both accurate and efficient by coupling quantization-aware training with a continuous architectural evolution: (1) In initialization, an over-parameterized ($2N$ -block) quantized backbone with learnable shortcuts improves representation capacity and provides an explicit importance signal for each block during warm-up. (2) In slimming, QSA progressively skips the least critical blocks according to these learned importance factors, yielding a compact N -block network while preserving training continuity. Compared with our conference method QuantSR [43], which performs one-shot slimming at a fixed training stage, QSA avoids abrupt topology changes that perturb optimization and invalidate previously learned representations, leading to a more stable path to the final efficient model.

3.4 QuantSR+: Slimming-guided Function-localized Distillation

3.4.1 Optimization Perturbations in Distillation

The high discreteness introduced by quantization interferes with the optimization of gradient-based SR models, not only due to the limited representation caused by compression in the forward propagation but also due to the inevitable errors brought by the gradient approximation. Due to the availability of a full-precision counterpart, distillation is considered an intuitive method to improve the performance of quantized models and has been widely used to optimize SR models. Specifically, quantization-aware distillation compares the outputs of a quantized SR student model and a full-precision teacher SR model to optimize the performance of the former. Moreover, when the student network is the full-precision counterpart of the teacher network, distillation can be performed at a finer granularity, such as layer-wise or block-wise (multi-layer) distillation.

However, the proposed QSA has an architecture that dynamically evolves during the optimization process, making it challenging to utilize existing quantization-aware distillation frameworks for SR models. After architectural changes,

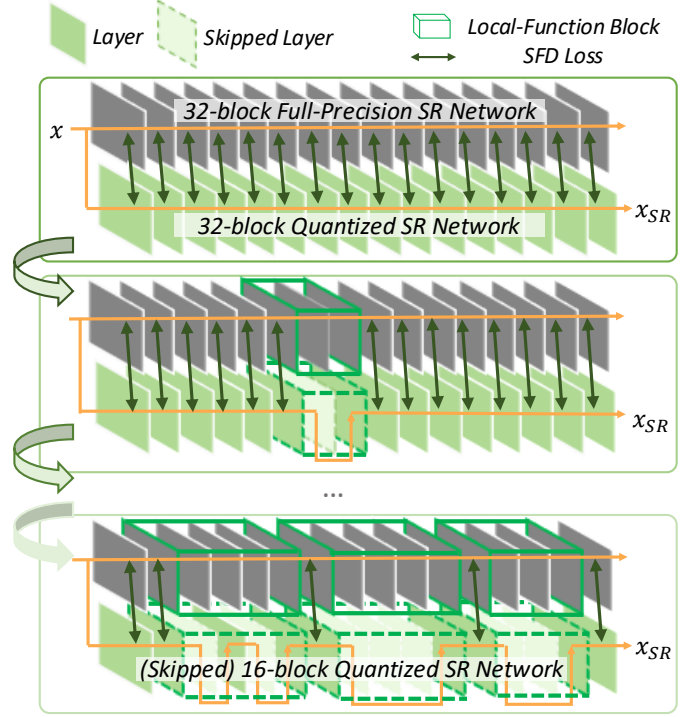


Fig. 5: SFD integrates different layers to form local functional blocks corresponding to full-precision and quantized SR models to accelerate the convergence of quantized SR models.

distillation can only be performed at the output positions of the SR model, or the full-precision counterpart of the evolved architecture needs to be retrained. This means that the training and optimization efficiency under these frameworks is severely limited. Therefore, we propose that QuantSR+ with QSA requires a new quantization-aware distillation method to enable universal and efficient optimization for quantized models in image SR tasks.

3.4.2 Slimming-guided Function-localized Distillation for Stable Convergence

We introduce the Slimming-guided Function-localized Distillation (SFD) to optimize dynamic quantized SR networks, which is shown in Fig. 5. SFD allows for the optimization process to exploit a powerful, full-size, full-precision SR teacher to supervise a slim, ultra-low-bit quantized student model, utilizing a function-localized strategy to accelerate the convergence of the quantized model.

Throughout the training process, the Quantized Slimming Architecture (QSA) evolves from an initial full-size ($2N$ blocks) structure to a slim (N blocks) final version. We first propose a foundational framework for the distillation of the quantized architecture, specifically the block-to-block correspondence distillation between the full-size teacher and student. Given the same representation dimensions and number of blocks, we directly compute the Mean Squared Error (MSE) loss at the block level to optimize the model:

$$\mathcal{L}_{\text{distill}}^{\text{init}} = \frac{1}{2N} \sum_{i=1}^{2N} \left\| \frac{\Phi_i^{\text{FP}}(x_i^{\text{FP}}) - \Phi_i^{\text{QSA}}(x_i)}{|\Phi_i^{\text{FP}}(x_i^{\text{FP}})|} \right\|_{\ell_2}^2, \quad (16)$$

where Φ_i^{FP} and Φ_i^{QSA} denote the output representation of the i -th block from full-precision and quantized SR models,

respectively, $\|\cdot\|_{\ell_2}$ denotes the ℓ_2 normalization function, and $|\cdot|$ denotes the cardinality function of the set, *i.e.*, the number of elements in the set.

After the onset of evolution, we propose a slimming-guided, function-localized distillation strategy between the full-size teacher and the slim student. The aim of this strategy is to establish a simple yet effective correspondence to leverage the quantized blocks surrounding the slimmed blocks to compensate for the local functionality of the slimmed blocks, allowing most of the blocks in the quantized SR model to be under stable supervision and optimization during evolution. Consider the first slimming of the initial quantized SR student. After skipping the i -th block, the supervision of the input (if any) and output of the i -th block is removed from the loss, retaining the distillation loss items established by the input of the $\{i-1\}$ -th block and the output of the $\{i+1\}$ -th block with the teacher model. This means that we expect the set of blocks $\Phi_{i-1}^{\text{QSA}}, \Phi_{i+1}^{\text{QSA}}$ in the quantized model to learn the corresponding functionality of the block set $\Phi_{i-1}^{\text{FP}}, \Phi_i^{\text{FP}}, \Phi_{i+1}^{\text{FP}}$ in the full-precision model, thereby producing similar outputs at $\{i+1\}$ -th block. Supervision of other blocks in the quantized model remains unchanged, allowing them to learn stably throughout the optimization process as long as they are not slimmed. The proposed SFD can be represented as follows:

$$\mathcal{L}_{\text{distill}}^{\text{SFD}} = \frac{1}{2N} \sum_{i=1}^{2N} \left[\Phi_i^{\text{QSA}} \in S \right] \cdot \left[\Phi_{i+1}^{\text{QSA}} \in S \right] \cdot \left\| \frac{\Phi_i^{\text{FP}}(\mathbf{x}_i^{\text{FP}}) - \Phi_i^{\text{QSA}}(\mathbf{x}_i)}{|\Phi_i^{\text{FP}}(\mathbf{x}_i^{\text{FP}})|} \right\|_2^2. \quad (17)$$

In the SFD for training optimization, the set of skipped blocks S dynamically changes (until the final optimized S^*), meaning that supervision is modified as the architecture evolves. However, for all non-adjacent skipped blocks currently within the set S , the supervision at their input and output positions does not change during optimization. This allows them to undergo stable optimization towards a consistent objective, enabling faster achievement of a highly accurate quantized SR model.

Considering the proposed SFD training strategy, we provide the overall training loss for QuantSR+. Given a training dataset $D = \{\mathcal{I}_{\text{LR}}^i, \mathcal{I}_{\text{HR}}^i\}_{i=1}^K$ consisting of K low-resolution inputs \mathcal{I}_{LR} and their corresponding high-resolution ground truths \mathcal{I}_{HR} , the traditional pixel loss \mathcal{L}^{PIX} for the quantized SR model \mathcal{M} can be expressed as:

$$\mathcal{L}^{\text{PIX}} = \frac{1}{K} \sum_{i=1}^K \|\mathcal{I}_{\text{HR}}^i - \mathcal{M}(\mathcal{I}_{\text{LR}}^i)\|_{\ell_1}. \quad (18)$$

This pixel loss is jointly optimized with the SFD loss to train the network as follows:

$$\mathcal{L} = \mathcal{L}^{\text{PIX}} + \lambda \mathcal{L}^{\text{SFD}}, \quad (19)$$

where λ is a balancing coefficient between the pixel loss and the SFD loss, empirically set to 1×10^{-4} .

With carefully designed quantizers, architectures, and optimization pipelines, QuantSR+ pushes the limits of accuracy and efficiency for quantized SR networks. Moreover, it can be universally applied to and improve backbones based on both convolution and attention mechanisms.

4 EXPERIMENT RESULTS

We follow the standard procedure for image SR by training on the DIV2K dataset [48] and evaluating on commonly used benchmark datasets, including Set5 [3], Set14 [59], B100 [40], Urban100 [21], and Manga109 [41]. We report the reconstruction accuracy of the comparison methods and our proposed QuantSR+ in terms of PSNR and SSIM [54] on the Y channel of the YCbCr color space. Additionally, we present both the savings of the storage usage and the computational complexity of the quantized SR models compared to their full-precision counterparts.

We apply our proposed quantization method to image SR models, including convolution-based and transformer-based SR architectures. For convolution-based models, we follow the approaches in DoReFa [65], PAMS [31], CADyQ [16], QuantSR [43], AdaBM [19], Granular-DQ [53], CABM [47], I²NQ [45], RefQSR [29], PTQ4SR [49], DAQ [18], and ODM [20], and we use the SRResNet backbone to construct the model. For transformer-based SR models, we quantize the lightweight version of SwinIR [33], comparing our QuantSR+ with QuantSR [43], ODM [20], and 2DQuant [38]. We also apply our method to diffusion-based SR backbones [52]. The implementation of these methods follows their papers [45], [65] and released codes [17], [32], [42], or follows results reported in their original papers directly [20], [47], [53]. All implemented models are trained under identical settings and pipelines to ensure consistency. We quantize the weights and activations in the body part of each model to 2, 4, or 8 bit-widths. We denote the w -bit weight and a -bit activation as w/a . For a fair comparison, QuantSR reports performance for variants with the same depth as the other networks, *i.e.*, 16 blocks for SRResNet and 4 blocks for SwinIR.

During the training process, we adopt the data augmentation techniques used in prior studies [33], [34], [43], [57], [62], including random rotations of 90°, 180°, and 270°, as well as horizontal flipping. The quantized SR models are trained for 300K iterations, with each training batch comprising 32 image patches, each with an input size of 64×64 . We optimize our model using the Adam optimizer [27], starting with an initial learning rate of 2e-4, which is halved after the 250K-th iteration. Notably, on SwinIR's W2A2, we aligned the training settings with the ODM [20], *i.e.*, 300K iterations with an initial learning rate of 1e-4, halved every 75K iterations, and we further present the comparative analysis of different strategies based on this case in Section 6.6.

4.1 Main Results

For our studies, we adopt two distinct architectures as the backbone models: SRResNet [28], a convolutional neural network (CNN) with 1,367K parameters for $\times 2$ upscaling and 1,515K parameters for $\times 4$, and SwinIR_S [33], a compact transformer-based model featuring 910K and 930K parameters for $\times 2$ and $\times 4$ scales, respectively. The quantized versions of our QuantSR+ are evaluated alongside established quantization approaches, including DoReFa [65], PAMS [31], CADyQ [16], QuantSR [43], AdaBM [19], Granular-DQ [53], CABM [47], I²NQ [45], ODM [20], RefQSR [29], PTQ4SR [49], DAQ [18], and 2DQuant [38].

For the convolution-based SRResNet, Table 1 reports quantitative results at $\times 2$ and $\times 4$ under 2-bit and 4-bit

Method	Scale	#Bit (w/a)	Set5		Set14		B100		Urban100		Manga109	
			PSNR	SSIM	PSNR	SSIM	PSNR	SSIM	PSNR	SSIM	PSNR	SSIM
Bicubic	$\times 2$	-/-	33.66	0.9299	30.24	0.8688	29.56	0.8431	26.88	0.8403	30.80	0.9339
SRResNet [28]	$\times 2$	32/32	38.00	0.9605	33.59	0.9171	32.19	0.8997	32.11	0.9282	38.56	0.9770
DoReFa [65]	$\times 2$	8/8	37.32	0.9520	32.90	0.8680	31.69	0.8504	30.32	0.8800	37.01	0.9450
CADyQ [16]	$\times 2$	8/8	37.79	0.9590	33.37	0.9150	32.02	0.8980	31.53	0.9230	38.06	0.9760
AdaBM [19]	$\times 2$	4/4MP	37.10	0.9550	32.85	0.9100	31.63	0.8910	30.48	0.9120	-	-
CABM [47]	$\times 2$	4/4MP	-	-	-	-	-	-	31.54	0.9230	-	-
Granular-DQ [53]	$\times 2$	4/4MP	-	-	-	-	-	-	31.94	0.9270	-	-
DoReFa [65]	$\times 2$	4/4	37.31	0.9510	32.48	0.9091	31.64	0.8901	30.18	0.8780	36.95	0.9440
PAMS [31]	$\times 2$	4/4	37.67	0.9588	33.19	0.9146	31.90	0.8966	31.10	0.9194	37.62	0.9740
CADyQ [16]	$\times 2$	4/4	37.58	0.9580	33.14	0.9140	31.87	0.8960	30.94	0.9170	37.31	0.9740
QuantSR [43]	$\times 2$	4/4	37.80	0.9597	33.35	0.9158	32.04	0.8979	31.46	0.9221	38.25	0.9762
PTQ4SR [49]	$\times 2$	4/4	36.49	0.9510	32.40	0.9040	31.36	0.8850	29.90	0.9040	-	-
I ² NQ [45] *	$\times 2$	4/4	37.94	0.9603	33.54	0.9168	32.10	0.8988	31.74	0.9250	38.48	0.9768
QuantSR+	$\times 2$	4/4	37.91	0.9602	33.52	0.9165	32.09	0.8986	31.75	0.9250	38.46	0.9767
QuantSR+*	$\times 2$	4/4	37.96	0.9605	33.60	0.9172	32.15	0.8990	31.79	0.9254	38.55	0.9770
DoReFa [65]	$\times 2$	2/2	36.91	0.9470	32.55	0.9071	31.41	0.8868	29.60	0.8740	36.13	0.9410
PAMS [31]	$\times 2$	2/2	34.04	0.8270	30.91	0.8751	30.11	0.8592	27.57	0.8400	31.79	0.9110
CADyQ [16]	$\times 2$	2/2	19.44	0.5610	18.51	0.4810	19.70	0.4760	17.97	0.4550	17.35	0.5830
QuantSR [43]	$\times 2$	2/2	37.57	0.9589	33.09	0.9136	31.84	0.8954	30.77	0.9149	37.60	0.9745
QuantSR+	$\times 2$	2/2	37.77	0.9596	33.32	0.9147	31.97	0.8968	31.25	0.9198	37.96	0.9756
Bicubic	$\times 4$	-/-	28.42	0.8104	26.00	0.7027	25.96	0.6675	23.14	0.6577	24.89	0.7866
SRResNet [28]	$\times 4$	32/32	32.16	0.8951	28.60	0.7822	27.58	0.7364	26.11	0.7870	30.46	0.9089
AdaBM [19]	$\times 4$	4/4MP	31.02	0.8600	27.87	0.7510	26.91	0.7000	25.11	0.7360	-	-
CABM [47]	$\times 4$	4/4MP	-	-	-	-	-	-	25.86	0.7780	-	-
RefQSR (δ -4bit) [29]	$\times 4$	4/4MP	-	-	-	-	-	-	25.90	0.7780	-	-
Granular-DQ [53]	$\times 4$	4/4MP	-	-	-	-	-	-	25.98	0.7830	-	-
DoReFa [65]	$\times 4$	4/4	29.57	0.8369	26.82	0.7352	26.47	0.6971	23.75	0.6898	27.89	0.8634
PAMS [31]	$\times 4$	4/4	31.59	0.8851	28.20	0.7725	27.32	0.7220	25.32	0.7624	28.86	0.8805
CADyQ [16]	$\times 4$	4/4	31.48	0.8830	28.05	0.7690	27.21	0.7240	25.09	0.7520	28.82	0.8840
PTQ4SR [49]	$\times 4$	4/4	31.15	0.8780	27.89	0.7630	27.15	0.7180	25.13	0.7530	-	-
QuantSR [43]	$\times 4$	4/4	32.00	0.8924	28.50	0.7799	27.52	0.7342	25.88	0.7807	30.15	0.9040
I ² NQ [45] *	$\times 4$	4/4	32.16	0.8948	28.53	0.7809	27.56	0.7357	25.95	0.7826	30.30	0.9062
QuantSR+	$\times 4$	4/4	32.13	0.8940	28.50	0.7804	27.53	0.7351	25.94	0.7825	30.30	0.9061
QuantSR+*	$\times 4$	4/4	32.17	0.8951	28.53	0.7810	27.60	0.7363	26.01	0.7832	30.35	0.9076
DoReFa [65]	$\times 4$	2/2	30.54	0.8610	27.50	0.7538	26.90	0.7098	24.44	0.7242	27.31	0.8502
PAMS [31]	$\times 4$	2/2	29.20	0.8239	26.61	0.7273	26.36	0.6934	23.58	0.6812	25.59	0.8012
CADyQ [16]	$\times 4$	2/2	19.67	0.5380	19.30	0.4740	19.80	0.4620	17.97	0.4360	17.30	0.5640
DAQ [18]	$\times 4$	2/2	31.67	-	28.26	-	27.32	-	25.39	-	-	-
QuantSR [43]	$\times 4$	2/2	31.30	0.8819	28.08	0.7694	27.23	0.7246	25.13	0.7537	28.81	0.8844
ODM [20]	$\times 4$	2/2	31.81	0.8880	28.32	0.7740	27.38	0.7300	25.54	0.7670	-	-
QuantSR+	$\times 4$	2/2	31.89	0.8908	28.37	0.7763	27.43	0.7308	25.58	0.7702	29.67	0.8974

TABLE 1: Quantitative results. SRResNet is used as the full-precision backbone. ‘ w/a ’ denotes the weight/activation bits, and ‘MP’ denotes the mixed-precision settings. * denotes the activation shifting and partition in [45].

quantization, with additional 8-bit references available at $\times 2$. In the ultra-low 2-bit setting, QuantSR+ consistently improves over the strongest prior fixed-precision baselines on all five benchmarks. On Set5, it improves PSNR/SSIM from 31.81/0.8880 (ODM) to 31.89/0.8908 at $\times 4$, corresponding to gains of 0.08dB/0.0028. Similar gains are also observed on Set14, B100, Urban100, and Manga109, demonstrating the robustness of QuantSR+ across different image contents and scaling factors. In the 4-bit setting, QuantSR+ remains highly competitive, while its enhanced variant QuantSR+*, obtained by incorporating the activation shifting and partition strategy from I²NQ [45], achieves the best overall performance. For example, QuantSR+* reaches 32.17dB/0.8951 at $\times 4$, even surpassing the full-precision SRResNet (32.16dB/0.8951 at $\times 4$). Compared with mixed-precision methods [19], [47], [53], QuantSR+* also shows clear advantages, e.g., exceeding Granular-DQ by 0.03dB on Urban100 at $\times 4$. These results demonstrate both the effectiveness of QuantSR+ in low-bit SR and its compatibility with other advanced techniques.

As for transformer-based models, our QuantSR+ approach effectively mitigates the accuracy gap caused by quantization (TABLE 2). For example, with the 2-bit quantization, QuantSR+ outperforms QuantSR [43] by a substantial margin in $\times 4$ scale, achieving gains of 0.17 dB in PSNR and 0.0015 in SSIM on Set5. We also compare with recent quantization methods that natively support the SR transformer, and our QuantSR+ significantly improves the accuracy, e.g., 1.81 dB PSNR over 2DQuant [38] and 0.29 dB over ODM [20] on Urban100 at $\times 4$ scale under the same 300K iterations.

We further verify the generalization ability of our QuantSR+ on diffusion-based SR backbones in Table 3. For example, 4-bit QuantSR+ achieves the best PSNR, SSIM, LPIPS, DISTs, and FID among all quantized baselines. Compared with QuantSR, it improves PSNR and SSIM by 0.06 dB and 0.0148, while reducing LPIPS, DISTs, and FID by 0.0238, 0.0118, and 9.62.

By integrating quantization with a dynamically optimized lightweight architecture, QuantSR+ achieves substantial com-

Method	Scale	#Bit (w/a)	Set5		Set14		B100		Urban100		Manga109	
			PSNR	SSIM	PSNR	SSIM	PSNR	SSIM	PSNR	SSIM	PSNR	SSIM
Bicubic	$\times 2$	-/-	33.66	0.9299	30.24	0.8688	29.56	0.8431	26.88	0.8403	30.80	0.9339
SwinIR_S [33]	$\times 2$	32/32	38.14	0.9611	33.86	0.9206	32.31	0.9012	32.76	0.9340	39.12	0.9783
2DQuant [38]	$\times 2$	4/4	37.87	0.9594	33.41	0.9161	32.02	0.8971	31.84	0.9251	38.31	0.9761
QuantSR [43]	$\times 2$	4/4	38.10	0.9604	33.65	0.9186	32.21	0.8998	32.20	0.9295	38.85	0.9774
QuantSR+	$\times 2$	4/4	38.08	0.9608	33.86	0.9207	32.20	0.8999	32.31	0.9302	38.89	0.9776
2DQuant [38]	$\times 2$	2/2	36.00	0.9497	31.98	0.9012	30.91	0.8810	28.62	0.8819	34.40	0.9602
QuantSR [43]	$\times 2$	2/2	37.55	0.9587	33.12	0.9143	31.89	0.8958	30.96	0.9172	37.61	0.9745
QuantSR+	$\times 2$	2/2	37.67	0.9591	33.25	0.9145	31.91	0.8960	31.06	0.9178	37.85	0.9750
Bicubic	$\times 4$	-/-	28.42	0.8104	26.00	0.7027	25.96	0.6675	23.14	0.6577	24.89	0.7866
SwinIR_S [33]	$\times 4$	32/32	32.44	0.8976	28.77	0.7858	27.69	0.7406	26.47	0.7980	30.92	0.9151
2DQuant [38]	$\times 4$	4/4	31.77	0.8867	28.30	0.7733	27.37	0.7278	25.71	0.7712	29.71	0.8972
ODM [20]	$\times 4$	4/4	32.17	0.8920	28.59	0.7810	27.56	0.7360	26.06	0.7850	-	-
QuantSR [43]	$\times 4$	4/4	32.18	0.8941	28.63	0.7822	27.59	0.7367	26.11	0.7871	30.49	0.9087
QuantSR+	$\times 4$	4/4	32.25	0.8944	28.65	0.7830	27.60	0.7376	26.18	0.7892	30.58	0.9096
2DQuant [38]	$\times 4$	2/2	29.53	0.8372	26.86	0.7322	26.46	0.6927	23.84	0.6912	26.07	0.8163
QuantSR [43]	$\times 4$	2/2	31.53	0.8845	28.16	0.7715	27.28	0.7274	25.26	0.7609	29.06	0.8898
ODM [20]	$\times 4$	2/2	31.67	0.8850	28.23	0.7720	27.33	0.7280	25.36	0.7620	-	-
QuantSR+	$\times 4$	2/2	31.70	0.8860	28.28	0.7731	27.37	0.7277	25.65	0.7695	29.69	0.8968

TABLE 2: Quantitative results. SwinIR-S is used as the full-precision backbone.

Method	Scale	#Bit (w/a)	PSNR \uparrow	SSIM \uparrow	LPIPS \downarrow	DISTS \downarrow	FID \downarrow	NIQE \downarrow	MUSIQ \uparrow	MANIQA \uparrow	CLIPQA \uparrow
StableSR [52]	$\times 4$	32/32	23.28	0.5733	0.3115	0.2049	24.55	4.7825	65.70	0.6171	0.6767
PAMS [31]	$\times 4$	4/4	23.11	0.5379	0.4225	0.2886	89.99	3.7643	60.02	0.5083	0.7213
QuantSR [43]	$\times 4$	4/4	23.37	0.5464	0.4203	0.2872	88.24	3.9060	58.27	0.4972	0.7176
QuantSR+	$\times 4$	4/4	23.43	0.5612	0.3965	0.2754	78.62	3.9905	57.52	0.4911	0.6942
PAMS [31]	$\times 4$	2/2	17.88	0.3080	0.8730	0.4106	198.69	8.6302	39.66	0.3552	0.1861
QuantSR [43]	$\times 4$	2/2	17.99	0.3127	0.8593	0.4102	193.29	8.2745	40.08	0.3536	0.1861
QuantSR+	$\times 4$	2/2	18.12	0.3155	0.8362	0.3965	176.50	8.1393	40.81	0.3669	0.1719

TABLE 3: Quantitative comparison on diffusion-based SR backbones under quantization on DIV2K-Val.

Method	Body	H/T	Factor	Params (K)	Ops (G)	Set5 (PSNR)	Hardware path	Latency	Bandwidth	Throughput
SRResNet	32/32	32/32	-	1,515 (0%)	90.1 (0%)	32.16	ZCU104 PS, ARM Cortex-A53	4.54 s	23 MB/s	0.22 FPS
ODM [20]	4/4	32/32	l	303 (\downarrow 80.0%)	20.2 (\downarrow 77.5%)	32.00		2.15 s	21 MB/s	0.47 FPS
QuantSR [43]	4/4	32/32	c	303 (\downarrow 80.0%)	20.2 (\downarrow 77.5%)	32.00	Body on PL + Head/Tail on PS	2.15 s	21 MB/s	0.47 FPS
QuantSR+	4/4	32/32	c	303 (\downarrow 80.0%)	20.2 (\downarrow 77.5%)	32.13		2.15 s	21 MB/s	0.47 FPS
QuantSR+	4/4	8/8	c	248 (\downarrow 83.6%)	15.0 (\downarrow 83.4%)	32.02	Body on PL + Head/Tail on PL	33 ms	6.2 MB/s	30.3 FPS
ODM [20]	2/2	32/32	l	161 (\downarrow 89.4%)	10.9 (\downarrow 87.9%)	31.81		2.13 s	21 MB/s	0.47 FPS
QuantSR [43]	2/2	32/32	c	161 (\downarrow 89.4%)	10.9 (\downarrow 87.9%)	31.30	Body on PL + Head/Tail on PS	2.13 s	21 MB/s	0.47 FPS
QuantSR+	2/2	32/32	c	161 (\downarrow 89.4%)	10.9 (\downarrow 87.9%)	31.89		2.13 s	21 MB/s	0.47 FPS
QuantSR+	2/2	8/8	c	108 (\downarrow 92.9%)	5.8 (\downarrow 93.7%)	31.76	Body on PL + Head/Tail on PL	24 ms	8.5 MB/s	41.7 FPS

TABLE 4: Efficiency comparison on SRResNet ($\times 4$, 16 residual blocks). The input size for calculating theoretical Ops is $3 \times 256 \times 256$. ‘‘Factor’’ denotes the scaling-factor granularity, where c and l indicate channel-wise and layer-wise scaling, respectively. Hardware metrics are evaluated on the AMD/Xilinx ZCU104 board with a ZU7EV FPGA using an LR input size of $3 \times 64 \times 64$ and an HR output size of $3 \times 256 \times 256$. PS and PL denote the processing system and programmable logic on the ZCU104 board, respectively. Bandwidth denotes the effective average off-chip DDR memory bandwidth, and throughput denotes the end-to-end frame processing rate measured on the complete deployment path. The rows with FP32 head/tail (H/T) follow the original QuantSR+ protocol, while the rows with INT8 head/tail correspond to a deployment-oriented, fully-integer FINN-style implementation.

pression while maintaining strong reconstruction accuracy. TABLE 4 reports both theoretical efficiency and practical hardware deployment results. Following PAMS [31], the original QuantSR+ protocol quantizes the high-level feature extraction layers, reducing Params/Ops by 80.0%/77.5% at 4-bit and 89.4%/87.9% at 2-bit under the theoretical complexity protocol with a $3 \times 256 \times 256$ input size, while outperforming representative layer-wise and channel-wise methods, i.e., ODM [20] and QuantSR [43]. Since the backbone and bit-width mainly determine Params and Ops, the original-protocol rows for ODM, QuantSR, and QuantSR+ share the same Params/Ops, and the resulting accuracy gains mainly stem from improved quantizer design, scaling strategy, and reconstruction capability. We further evaluate QuantSR+

on the AMD/Xilinx ZCU104 board with a ZU7EV FPGA, using an LR input size of $3 \times 64 \times 64$ and an HR output size of $3 \times 256 \times 256$. With FP32 head/tail and a low-bit body, QuantSR+ achieves about $2.1 \times$ end-to-end speedup and 0.47 FPS throughput. With INT8 head/tail and a fully programmable-logic FINN-style dataflow implementation, the deployment-oriented W4A4 and W2A2 QuantSR+ implementations achieve 33 ms and 24 ms latency, corresponding to $138 \times$ and $189 \times$ system-level speedup, respectively. The corresponding end-to-end throughput reaches 30.3 FPS and 41.7 FPS, with effective average off-chip bandwidths of 6.2 MB/s and 8.5 MB/s. More detailed efficiency analysis is provided in Section 6.1 and Section 6.2.

Method	Scale	#Bit (w/a)	Set5		Set14		B100		Urban100		Manga109	
			PSNR	SSIM	PSNR	SSIM	PSNR	SSIM	PSNR	SSIM	PSNR	SSIM
SRResNet	×4	32/32	32.16	0.8951	28.60	0.7822	27.58	0.7364	26.11	0.7870	30.46	0.9089
Vanilla (DoReFa)	×4	2/2	30.54	0.8610	27.50	0.7538	26.90	0.7098	24.44	0.7242	27.31	0.8502
RBD	×4	2/2	30.75	0.8686	27.78	0.7514	26.99	0.7034	25.06	0.7394	28.46	0.8722
QSA	×4	2/2	31.01	0.8738	27.95	0.7573	27.11	0.7095	25.25	0.7476	28.80	0.8790
SFD	×4	2/2	31.21	0.8776	28.07	0.7616	27.20	0.7139	25.39	0.7538	29.07	0.8840
RBD+QSA	×4	2/2	31.45	0.8819	28.22	0.7667	27.31	0.7192	25.51	0.7616	29.41	0.8901
QuantSR+	×4	2/2	31.89	0.8908	28.37	0.7763	27.43	0.7308	25.58	0.7702	29.67	0.8974

TABLE 5: Ablation results (×4 scale) for Redistribution-driven Bit Determination (RBD), Quantized Slimmable Architecture (QSA), and Slimming-guided Function-localized Distillation (SFD) in QuantSR+ under the 2-bit setting.

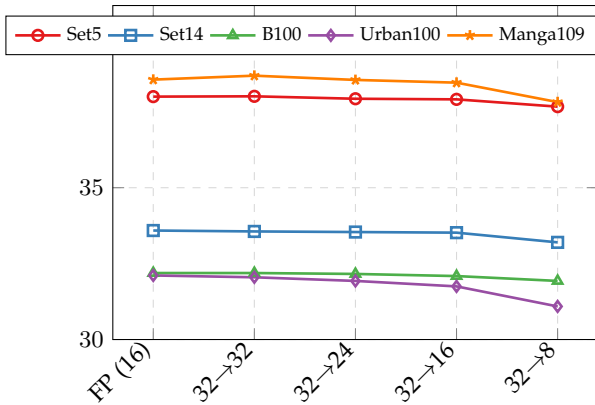


Fig. 6: QSA ablation results (PSNR) for different block configurations (×2 Scale, 4/4-bit). 16 (FP) means a 16 block model with 32-bit; others are 4/4-bit models quantized by QuantSR+.

Method	Scale	#Bit (w/a)	Set5		Set14	
			PSNR	SSIM	PSNR	SSIM
SRResNet [28]	×2	32/32	38.00	0.9605	33.59	0.9171
QuantSR+	×2	1/1	36.66	0.9548	32.39	0.9069
SRResNet [28]	×4	32/32	32.16	0.8951	28.60	0.7822
QuantSR+	×4	1/1	30.32	0.8604	27.40	0.7505

TABLE 6: 1/1-bit quantitative results on SRResNet.

4.2 Ablation Results

To demonstrate the effectiveness of the techniques in QuantSR+, we perform detailed ablation studies on RBD, QSA, and SFD. Our study is based on the SRResNet [28] backbone network, and uses the DoReFa quantization method as the vanilla quantized SR baseline model [65]. We then construct ablation studies for each technique based on the vanilla method. The experimental results are shown in TABLE 5, where we report the PSNR/SSIM values on five benchmark datasets.

As shown in TABLE 5, the effectiveness of RBD, QSA, and SFD is evaluated separately under the 2-bit W2A2 setting. Compared with the vanilla DoReFa model, RBD improves PSNR on all five benchmarks by 0.09-1.15 dB; for SSIM, it brings clear gains on Set5, Urban100, and Manga109, while the Set14 and B100 SSIM values are slightly lower than the vanilla baseline by 0.0024 and 0.0064, respectively. QSA also yields stable PSNR gains of 0.21-1.49 dB, while its SSIM improves by 0.0035-0.0288 across four benchmarks and shows only a marginal 0.0003 drop on B100, demonstrating that the slimmer architecture largely preserves reconstruction quality while reducing computational and memory costs. We further

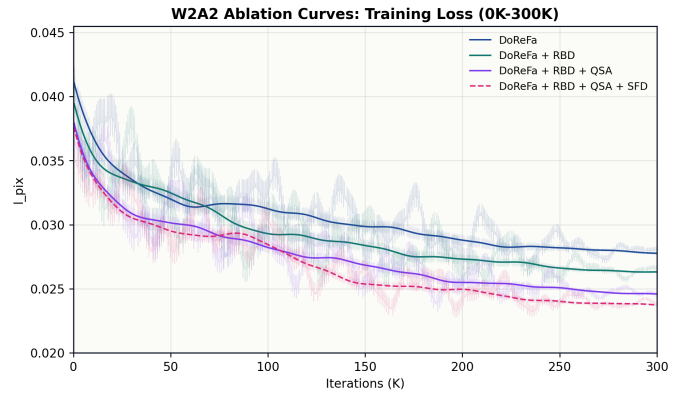


Fig. 7: W2A2 ablation curves of training loss on SRResNet ×4. The translucent curves denote the original per-iteration losses, and the solid/dashed curves denote the smoothed trends. Lower and smoother trajectories indicate more stable optimization.

investigate the impact of different block configurations under QSA (Fig. 6): our 4/4-bit quantized models maintain consistent performance even as we gradually reduce the block count from 32 to 24, then to 16, and finally to 8. Specifically, on Set5, the PSNR only slightly drops from 38.01 dB (32→32) to 37.67 dB (32→8). In particular, the 16-block configuration adapted by our QuantSR+ strikes a favorable balance between performance preservation and computational efficiency. This validates that QSA effectively preserves reconstruction quality while achieving significant model compression. Meanwhile, SFD further boosts reconstruction quality without changing the inference topology, and achieves the best results among the three individual variants, with improvements of 0.30-1.76 dB in PSNR and 0.0041-0.0338 in SSIM over the vanilla baseline. When all components are combined, QuantSR+ further improves over the vanilla baseline by 0.53-2.36 dB in PSNR and 0.0210-0.0472 in SSIM, confirming that the three components make effective and complementary contributions. We put more detailed results in Section 6.3.

Fig. 7 provides empirical evidence for the improved optimization stability claimed in the method section. Under the challenging W2A2 setting, the vanilla DoReFa baseline exhibits a higher and more fluctuating loss trajectory, while each proposed component progressively improves the convergence behavior. The resulting full QuantSR+ variant achieves the lowest and smoothest loss curve, with a clear advantage from about 50K to 300K iterations. These observations are consistent with our design motivation that

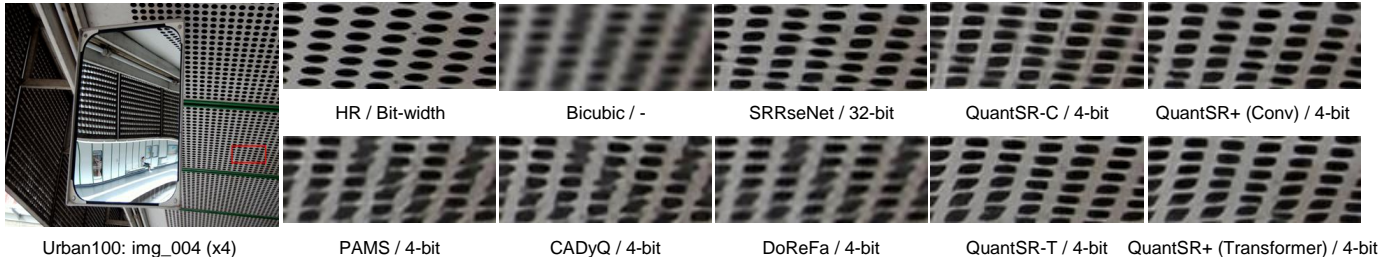


Fig. 8: Visualization ($\times 4$) for quantized SR models in terms of 4-bit setting.

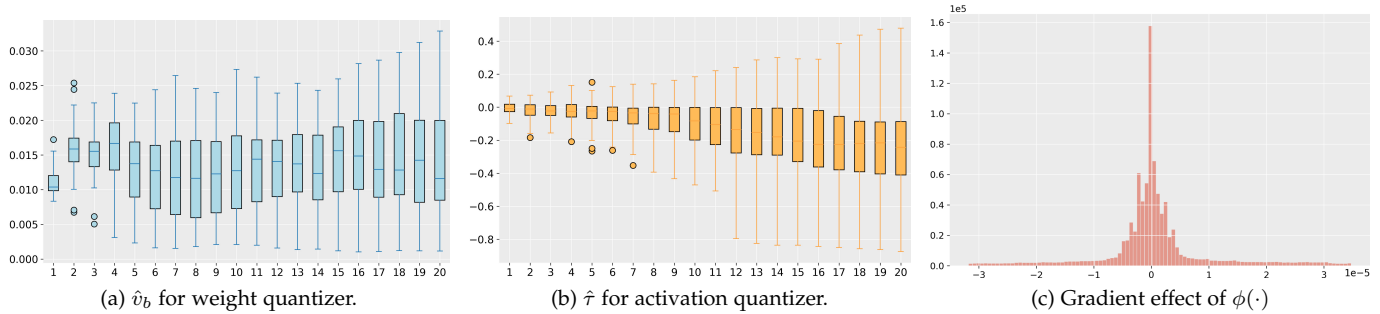


Fig. 9: The statistics of operator parameters in QuantSR+. The visualizations demonstrate the improvement in representation from quantized operators in forward and backward propagation.

QuantSR+ improves stability jointly from the operator, architecture, and optimization levels. More detailed convergence analyses are provided in Section 6.4.

We also present the model performance at ultra-low 1-bit (TABLE 6). Our specially designed RBD for multi-bit fine-grained optimization struggles to perform effectively at 1-bit because it cannot fully leverage cooperation among multiple bits to optimize performance. Therefore, the co-design of quantizer formulas, training strategies, and network architectures specifically for a single bit is a promising direction for future research.

4.3 Visualization Results

Fig. 8 presents more qualitative results of different methods at a $\times 4$ scale, focusing on 4-bit quantization. Our method, QuantSR+, is evaluated against existing quantization approaches, including DoReFa [65], PAMS [31], CADyQ [16], and QuantSR [43]. Both SRResNet- and SwinIR-based quantized variants of QuantSR and QuantSR+ are included in the comparison. Our results demonstrate that QuantSR+ is more effective in preserving structural details and minimizing blurring artifacts compared to other quantization techniques. Notably, the visual gap between our quantized model and the full-precision version is minimal, reinforcing the quantitative findings in TABLE 1 and TABLE 2 and further validating the effectiveness of QuantSR+.

Fig. 9 provides a statistical analysis of the learnable parameters and functional behavior of our RBD throughout the training process, recorded at every 100 iterations. We analyze key variables in our quantization functions, including \hat{v}_b from the activation quantizer, $\hat{\tau}$ from the weight quantizer, and the gradient effect of the activation transformation function $\phi(\cdot)$. Fig. 9 (a) and (b) reveal that these learnable parameters start with similar values but gradually diverge over training,

indicating that the QuantSR+ quantizer becomes more adaptive and effectively compensates for information loss due to discretization. In Fig. 9 (c), we examine the gradient behavior induced by the transformation function $\phi(\cdot)$ during back-propagation. While the forward propagation results and training stability remain unaffected, the gradient adjustments introduced by this function play a critical role in guiding optimization. This contribution significantly enhances the training dynamics of QuantSR+, leading to improved overall performance.

5 CONCLUSION

This paper introduces QuantSR+, a novel quantized image SR network designed to address the accuracy and efficiency challenges in low-bit SR models. Our proposed network features three key innovations: Redistribution-driven Bit Determination (RBD), which enhances the representational capability of quantization operators; Quantized Slimmable Architecture (QSA), which enables progressive structural evolution to push accuracy beyond full-precision limits; and Slimming-guided Function-localized Distillation (SFD), which mitigates quantization-induced errors and accelerates convergence. We demonstrate that QuantSR+ surpasses existing quantized SR networks and general quantization methods with SOTA results across various bit widths and evaluation benchmarks, and achieves up to 88% computation and storage savings at 2-bit highlighting its computational efficiency. Finally, QuantSR+ shows comprehensive accuracy and efficiency gains across both convolutional and transformer-based architectures, demonstrating its versatility and broad applicability. The QuantSR+ framework opens up new possibilities for the integration of advanced image SR networks via low-bit quantization in real-time scenarios, such as resource-constrained mobile and embedded devices.

ACKNOWLEDGMENTS

This work is supported by the National Natural Science Foundation of China (62501386), CCF-Tencent Rhino-Bird Open Research Fund, CAAI-Tencent Rhino-Bird Open Research Fund, and the Swiss National Science Foundation (SNSF) project 200021E_219943 Neuromorphic Attention Models for Event Data (NAMED). This work is supported by the fundamental research funds for the central universities, sponsored by the AI Hundred Schools Program, and carried out using the Ascend AI technology stack.

REFERENCES

- [1] Namhyuk Ahn, Byungkon Kang, and Kyung-Ah Sohn. Fast, accurate, and lightweight super-resolution with cascading residual network. In *ECCV*, 2018.
- [2] Yoshua Bengio, Nicholas Léonard, and Aaron Courville. Estimating or propagating gradients through stochastic neurons for conditional computation. *arXiv preprint arXiv:1308.3432*, 2013.
- [3] Marco Bevilacqua, Aline Roumy, Christine Guillemot, and Marie Line Alberi-Morel. Low-complexity single-image super-resolution based on nonnegative neighbor embedding. In *BMVC*, 2012.
- [4] Hanlin Chen, Li’An Zhuo, Baochang Zhang, Xiawu Zheng, Jianzhuang Liu, David Doermann, and Rongrong Ji. Binarized neural architecture search. *AAAI 2020 - 34th AAAI Conference on Artificial Intelligence*, pages 10526–10533, 2020.
- [5] Jungwook Choi, Zhuo Wang, Swagath Venkataramani, Pierce I-Jen Chuang, Vijayalakshmi Srinivasan, and Kailash Gopalakrishnan. PACT: Parameterized Clipping Activation for Quantized Neural Networks. *arXiv preprint arXiv:1805.06085*, pages 1–15, 2018.
- [6] Jungwook Choi, Zhuo Wang, Swagath Venkataramani, Pierce I-Jen Chuang, Vijayalakshmi Srinivasan, and Kailash Gopalakrishnan. Pact: Parameterized clipping activation for quantized neural networks. *arXiv preprint arXiv:1805.06085*, 2018.
- [7] Yoni Choukroun, Eli Kravchik, Fan Yang, and Pavel Kisilev. Low-bit quantization of neural networks for efficient inference. In *ICCVW*, 2019.
- [8] Xiangxiang Chu, Bo Zhang, Hailong Ma, Ruijun Xu, and Qingyuan Li. Fast, accurate and lightweight super-resolution with neural architecture search. *arXiv preprint arXiv:1901.07261*, 2019.
- [9] Zhen Dong, Zhewei Yao, Amir Gholami, Michael Mahoney, and Kurt Keutzer. HAWQ: Hessian aware quantization of neural networks with mixed-precision. In *Proceedings of the IEEE International Conference on Computer Vision*, 2019.
- [10] Alexey Dosovitskiy, Lucas Beyer, Alexander Kolesnikov, Dirk Weisensee, Xiaohua Zhai, Thomas Unterthiner, Mostafa Dehghani, Matthias Minderer, Georg Heigold, Sylvain Gelly, et al. An image is worth 16x16 words: Transformers for image recognition at scale. *arXiv preprint arXiv:2010.11929*, 2020.
- [11] Amir Gholami, Sehoon Kim, Zhen Dong, Zhewei Yao, Michael W. Mahoney, and Kurt Keutzer. A Survey of Quantization Methods for Efficient Neural Network Inference. *Low-Power Computer Vision*, pages 291–326, 3 2022.
- [12] Yong Guo, Jingdong Wang, Qi Chen, Jiezhong Cao, Zeshuai Deng, Yanwu Xu, Jian Chen, and Minghui Tan. Towards lightweight super-resolution with dual regression learning. *IEEE Transactions on Pattern Analysis and Machine Intelligence*, 2024.
- [13] B. Hassibi and D. G. Stork. Second order derivatives for network pruning: Optimal brain surgeon. In *NeurIPS*, 1993.
- [14] Zhibin He, Tao Dai, Jian Lu, Yong Jiang, and Shu-Tao Xia. Fkd: Feature-affinity based knowledge distillation for efficient image super-resolution. In *ICIP*, 2020.
- [15] Geoffrey Hinton, Oriol Vinyals, and Jeff Dean. Distilling the knowledge in a neural network. In *NeurIPS Workshop*, 2014.
- [16] Cheun Hong, Sungyong Baik, Heewon Kim, Seungjun Nah, and Kyoung Mu Lee. Cadyq: Content-aware dynamic quantization for image super-resolution. In *ECCV*, 2022.
- [17] Cheun Hong, Sungyong Baik, Heewon Kim, Seungjun Nah, and Kyoung Mu Lee. Cadyq, 05 2023.
- [18] Cheun Hong, Heewon Kim, Sungyong Baik, Junghun Oh, and Kyoung Mu Lee. Daq: Channel-wise distribution-aware quantization for deep image super-resolution networks. In *WACV*, 2022.
- [19] Cheun Hong and Kyoung Mu Lee. Adabm: On-the-fly adaptive bit mapping for image super-resolution. In *Proceedings of the IEEE/CVF Conference on Computer Vision and Pattern Recognition*, pages 2641–2650, 2024.
- [20] Cheun Hong and Kyoung Mu Lee. Overcoming distribution mismatch in quantizing image super-resolution networks. In *European Conference on Computer Vision*, pages 380–396. Springer, 2024.
- [21] Jia-Bin Huang, Abhishek Singh, and Narendra Ahuja. Single image super-resolution from transformed self-exemplars. In *CVPR*, 2015.
- [22] Itay Hubara, Yury Nahshan, Yair Hanani, Ron Banner, and Daniel Soudry. Accurate post training quantization with small calibration sets. In *ICML*, 2021.
- [23] Zheng Hui, Xinbo Gao, Yunchu Yang, and Xiumei Wang. Lightweight image super-resolution with information multi-distillation network. In *ACM MM*, 2019.
- [24] Andrey Ignatov, Radu Timofte, Maurizio Denna, Abdel Younes, Ganzorig Gankhuyag, Jingang Huh, Myeong Kyun Kim, Kihwan Yoon, Hyeon-Cheol Moon, Seunggho Lee, et al. Efficient and accurate quantized image super-resolution on mobile npus, mobile ai & aim 2022 challenge: report. In *ECCVW*, 2022.
- [25] Divyansh Jhunjhunwala, Advait Gadhikar, Gauri Joshi, and Yonina C Eldar. Adaptive quantization of model updates for communication-efficient federated learning. In *ICASSP*, 2021.
- [26] Jiwon Kim, Jung Kwon Lee, and Kyoung Mu Lee. Deeply-recursive convolutional network for image super-resolution. In *CVPR*, 2016.
- [27] Diederik Kingma and Jimmy Ba. Adam: A method for stochastic optimization. In *ICLR*, 2015.
- [28] Christian Ledig, Lucas Theis, Ferenc Huszár, Jose Caballero, Andrew Cunningham, Alejandro Acosta, Andrew Aitken, Alykhan Tejani, Johannes Totz, Zehan Wang, and Wenzhe Shi. Photo-realistic single image super-resolution using a generative adversarial network. In *CVPR*, 2017.
- [29] Hongjae Lee, Jun-Sang Yoo, and Seung-Won Jung. Refqsr: Reference-based quantization for image super-resolution networks. *IEEE Transactions on Image Processing*, 33:2823–2834, 2024.
- [30] Wonkyung Lee, Junghyup Lee, Dohyung Kim, and Bumsuh Ham. Learning with privileged information for efficient image super-resolution. In *ECCV*, 2020.
- [31] Huixia Li, Chenqian Yan, Shaohui Lin, Xiawu Zheng, Baochang Zhang, Fan Yang, and Rongrong Ji. Pams: Quantized super-resolution via parameterized max scale. In *ECCV*, 2020.
- [32] Huixia Li, Chenqian Yan, Shaohui Lin, Xiawu Zheng, Baochang Zhang, Fan Yang, and Rongrong Ji. Pams, 05 2023.
- [33] Jingyun Liang, Jiezhong Cao, Guolei Sun, Kai Zhang, Luc Van Gool, and Radu Timofte. Swinir: Image restoration using swin transformer. In *ICCVW*, 2021.
- [34] Bee Lim, Sanghyun Son, Heewon Kim, Seungjun Nah, and Kyoung Mu Lee. Enhanced deep residual networks for single image super-resolution. In *CVPRW*, 2017.
- [35] Xinqi Lin, Jingwen He, Ziyan Chen, Zhaoyang Lyu, Bo Dai, Fanghua Yu, Wanli Ouyang, Yu Qiao, and Chao Dong. Diffbir: Towards blind image restoration with generative diffusion prior. *ECCV*, 2024.
- [36] Anran Liu, Yihao Liu, Jinjin Gu, Yu Qiao, and Chao Dong. Blind image super-resolution: A survey and beyond. *IEEE transactions on pattern analysis and machine intelligence*, 45(5):5461–5480, 2022.
- [37] Jingyu Liu, Qiong Wang, Dunbo Zhang, and Li Shen. Super-resolution model quantized in multi-precision. *Electronics*, 10(17):2176, 2021.
- [38] Kai Liu, Haotong Qin, Yong Guo, Xin Yuan, Linghe Kong, Guihai Chen, and Yulun Zhang. 2dquant: Low-bit post-training quantization for image super-resolution. *Advances in Neural Information Processing Systems*, 37:71068–71084, 2025.
- [39] Denis Makhov, Ruslan Ostapets, Irina Zhelavskaya, Dehua Song, and Kirill Solodskikh. Towards robust full low-bit quantization of super resolution networks. In *European Conference on Computer Vision*, pages 182–198. Springer, 2024.
- [40] David Martin, Charles Fowlkes, Doron Tal, and Jitendra Malik. A database of human segmented natural images and its application to evaluating segmentation algorithms and measuring ecological statistics. In *ICCV*, 2001.
- [41] Yusuke Matsui, Kota Ito, Yuji Aramaki, Azuma Fujimoto, Toru Ogawa, Toshihiko Yamasaki, and Kiyoharu Aizawa. Sketch-based manga retrieval using manga109 dataset. *Multimedia Tools and Applications*, 2017.
- [42] Haotong Qin, Yulun Zhang, Yifu Ding, Xianglong Liu, Martin Danelljan, Fisher Yu, et al. Quantsr, 10 2023.
- [43] Haotong Qin, Yulun Zhang, Yifu Ding, Xianglong Liu, Martin Danelljan, Fisher Yu, et al. Quantsr: accurate low-bit quantization for efficient image super-resolution. *Advances in Neural Information Processing Systems*, 36, 2024.
- [44] Jian-Nan Su, Min Gan, Guang-Yong Chen, Jia-Li Yin, and CL Philip Chen. Global learnable attention for single image super-resolution.

- IEEE Transactions on Pattern Analysis and Machine Intelligence*, 45(7):8453–8465, 2022.
- [45] Liting Sun, Jingwei Xin, Keyu Li, Jie Li, Nannan Wang, and Xinbo Gao. I²nq: Inter and intra nonuniform quantization for single image super-resolution. *IEEE Transactions on Neural Networks and Learning Systems*, 2024.
- [46] Wanjie Sun and Zhenzhong Chen. Learning many-to-many mapping for unpaired real-world image super-resolution and downscaling. *IEEE Transactions on Pattern Analysis and Machine Intelligence*, 2024.
- [47] Senmao Tian, Ming Lu, Jiaming Liu, Yandong Guo, Yurong Chen, and Shunli Zhang. Cabm: Content-aware bit mapping for single image super-resolution network with large input. In *Proceedings of the IEEE/CVF Conference on Computer Vision and Pattern Recognition*, pages 1756–1765, 2023.
- [48] Radu Timofte, Eirikur Agustsson, Luc Van Gool, Ming-Hsuan Yang, Lei Zhang, Bee Lim, Sanghyun Son, Heewon Kim, Seungjun Nah, Kyoung Mu Lee, et al. Ntire 2017 challenge on single image super-resolution: Methods and results. In *CVPRW*, 2017.
- [49] Zhijun Tu, Jie Hu, Hanting Chen, and Yunhe Wang. Toward accurate post-training quantization for image super resolution. In *Proceedings of the IEEE/CVF Conference on Computer Vision and Pattern Recognition*, pages 5856–5865, 2023.
- [50] Hu Wang, Peng Chen, Bohan Zhuang, and Chunhua Shen. Fully quantized image super-resolution networks. In *ACM MM*, 2021.
- [51] Hailing Wang, Jianglin Lu, Yitian Zhang, and Yun Fu. Outlier-aware post-training quantization for image super-resolution. In *Proceedings of the IEEE/CVF International Conference on Computer Vision*, pages 16175–16184, 2025.
- [52] Jianyi Wang, Zongsheng Yue, Shangchen Zhou, Kelvin CK Chan, and Chen Change Loy. Exploiting diffusion prior for real-world image super-resolution. *International Journal of Computer Vision*, 132(12):5929–5949, 2024.
- [53] Mingshen Wang, Zhao Zhang, Feng Li, Ke Xu, Kang Miao, and Meng Wang. Thinking in granularity: Dynamic quantization for image super-resolution by intriguing multi-granularity clues. In *Proceedings of the AAAI Conference on Artificial Intelligence*, volume 39, pages 7826–7834, 2025.
- [54] Zhou Wang, Alan C Bovik, Hamid R Sheikh, and Eero P Simoncelli. Image quality assessment: from error visibility to structural similarity. *TIP*, 2004.
- [55] Hao Wu, Patrick Judd, Xiaojie Zhang, Mikhail Isaev, and Paulius Micikevicius. Integer quantization for deep learning inference: Principles and empirical evaluation. *arXiv preprint arXiv:2004.09602*, 2020.
- [56] Rongyuan Wu, Lingchen Sun, Zhiyuan Ma, and Lei Zhang. One-step effective diffusion network for real-world image super-resolution. *NIPS*, 2024.
- [57] Jingwei Xin, Nannan Wang, Xinrui Jiang, Jie Li, Heng Huang, and Xinbo Gao. Binarized neural network for single image super resolution. In *ECCV*, 2020.
- [58] Zongsheng Yue, Kang Liao, and Chen Change Loy. Arbitrary-steps image super-resolution via diffusion inversion. *arXiv preprint arXiv:2412.09013*, 2024.
- [59] Roman Zeyde, Michael Elad, and Matan Protter. On single image scale-up using sparse-representations. In *Proc. 7th Int. Conf. Curves Surf.*, 2010.
- [60] He Zhang and Vishal M Patel. Densely connected pyramid dehazing network. In *CVPR*, 2018.
- [61] Jingyi Zhang, Ziwei Wang, Haoyu Wang, Jie Zhou, and Jiwen Lu. Anycost network quantization for image super-resolution. *IEEE Transactions on Image Processing*, 33:2279–2292, 2024.
- [62] Kai Zhang, Wangmeng Zuo, and Lei Zhang. Learning a single convolutional super-resolution network for multiple degradations. In *CVPR*, 2018.
- [63] Yulun Zhang, Yapeng Tian, Yu Kong, Bineng Zhong, and Yun Fu. Residual dense network for image restoration. *IEEE transactions on pattern analysis and machine intelligence*, 43(7):2480–2495, 2021.
- [64] Yulun Zhang, Huan Wang, Can Qin, and Yun Fu. Aligned structured sparsity learning for efficient image super-resolution. In *NeurIPS*, 2021.
- [65] Shuchang Zhou, Yuxin Wu, Zekun Ni, Xinyu Zhou, He Wen, and Yuheng Zou. Dorefa-net: Training low bitwidth convolutional neural networks with low bitwidth gradients. *arXiv preprint arXiv:1606.06160*, 2016.



Haotong Qin is a Postdoctoral Researcher at the Center for Project-Based Learning (PBL) D-ITET at ETH Zürich. He was a Ph.D. student in the State Key Laboratory of Complex and Critical Software Environment at Beihang University. He obtained a B.Eng degree in computer science and engineering from Beihang University. His research interests include model compression and deployment toward efficient deep learning in real-world scenarios. He has published 35 papers in top-tier journals and conferences, such as IEEE TPAMI, IEEE TNNLS, IJCV, ICML, NeurIPS, ICLR, and CVPR. He serves as Guest Editor for Neural Networks, Area Chair in BMVC, and Reviewer for IEEE TPAMI, IEEE TIP, IEEE TNNLS, CVPR, etc.



Jinyang Guo is an Assistant Professor at the State Key Laboratory of Complex & Critical Software Environment, Institute of Artificial Intelligence, Beihang University, China. Previously, he obtained his B.Eng (Hons1) degree from the School of Electrical and Telecommunication, The University of New South Wales, Australia, and later received his Ph.D. from the School of Electrical and Information Engineering, The University of Sydney. His research interests include efficient and scalable AI computing (e.g., model-efficiency, data-efficiency, label-efficiency), neuromorphic computing (e.g., spiking neural networks), and AI4Science (e.g., AI for quantum computing).



Xudong Ma received the B.E. degree in Network Engineering from the University of Electronic Science and Technology of China. He is currently working toward a PhD degree in the State Key Laboratory of Complex and Critical Software Environment at Beihang University under the supervision of Prof. Jie Luo. His research interests include model compression, knowledge graphs, and language models. He has published papers in NeurIPS, ICML, IJCAI, and IEEE TNNLS.



Michele Magno is currently a Privatdozent with the Department of Information Technology and Electrical Engineering (D-ITET), ETH Zürich, where he has been leading the D-ITET Center for project-based learning since 2020. He is also a Fellow of IEEE. He received master's and Ph.D. degrees in electronic engineering from the University of Bologna, Bologna, Italy, in 2004 and 2010, respectively. Since 2013, he has been with ETH Zürich, Zürich, Switzerland, and has become a Visiting Lecturer or a Professor at several universities, namely, the University of Nice Sophia, Nice, France; Enssat Lannion, Lannion, France; the University of Bologna, Bologna, Italy; and Mid University Sweden, Sundsvall, Sweden; where is a Full Visiting Professor with the Department of Electrical Engineering. He has authored more than 300 papers in international journals and conferences. His current research interests include smart sensing, low-power machine learning, wireless sensor networks, wearable devices, energy harvesting, low-power management techniques, and extension of the lifetime of battery-operated devices. He is an ACM Member. Some of his publications were awarded Best Paper awards at several IEEE conferences. He also received awards for industrial projects or patents.



Jie Luo is now an Associate Professor in the State Key Laboratory of Complex and Critical Software Environment, School of Computer Science and Engineering, Beihang University. He received a B.S. degree from the School of Mathematical Sciences, Peking University, in 2003. He received a Ph.D. from Beihang University in 2012 under the supervision of Prof. Wei Li and visited the University of Washington as a joint PhD student. His research interests include logic foundations for computer science, knowledge engineering, and crowd intelligence. He has published over 40 papers in top conferences and journals in artificial intelligence and information security, such as NeurIPS, ICML, CVPR, IJCAI, BiBM, KSEM, and PR.



Xianglong Liu is currently a Professor, serves as the vice dean of the School of Computer Science and Engineering at Beihang University, and is also the deputy director of the State Key Laboratory of Complex and Critical Software Environment. He received his B.S. and Ph.D. degrees under the supervision of Prof. Wei Li and visited the DVMM Lab at Columbia University as a joint PhD student supervised by Prof. Shih-Fu Chang. He is the recipient of the China National Excellent Youth Science Fund. He has published over 100 papers in top conferences/journals in artificial intelligence and information security, such as NeurIPS, ICLR, CVPR, ICCV, CSS, and IJCV. He serves as Associate Editor and Guest for several SCI journals like Pattern Recognition and IET Image Processing, and as Promotion Editor for journals like Frontiers of Computer Science and Acta Aeronautica et Astronautica Sinica. He serves as Area Chair in top conferences such as AAAI and ACM MM and has frequently organized workshops and competitions in conferences like CVPR, IJCAI, and AAAI.



Yulun Zhang received a B.E. degree from the School of Electronic Engineering, Xidian University, China, in 2013, an M.E. degree from the Department of Automation, Tsinghua University, China, in 2017, and a Ph.D. degree from the Department of ECE, Northeastern University, USA, in 2021. He is an associate professor at Shanghai Jiao Tong University, Shanghai, China. He was a postdoctoral researcher at the Computer Vision Lab, ETH Zürich, Switzerland. His research interests include image/video restoration and synthesis, biomedical image analysis, model compression, multimodal computing, large language models, and computational imaging. He is/was an Area Chair for CVPR, ICCV, ECCV, NeurIPS, ICML, ICLR, IJCAI, ACM MM, and a Senior Program Committee (SPC) member for IJCAI and AAAI.